

A&A manuscript no.
(will be inserted by hand later)

Your thesaurus codes are:
13.18.1, 11.10.1, 11.17.3, 11.17.4 Cygnus A, 11.17.4 3C 309.1, 11.17.4 3C 345

ASTRONOMY
AND
ASTROPHYSICS
27.9.2017

Ultracompact jets in AGN

A.P. Lobanov

Max-Planck-Institut für Radioastronomie, Auf dem Hügel 69, D-53121 Bonn, Germany

Received August 15; accepted September 24, 1997

Abstract. We study the properties of ultracompact jets in several prominent radio sources (Cygnus A, 3C 309.1, 3C 345, 3C 395, 4C 39.25, and 1038+528 A), using the frequency dependence of observed position of the optically thick jet core. Frequency dependent offsets of the core positions are used for calculating the luminosities, magnetic fields, and geometrical properties of the jets. Opacity effects are studied, for both synchrotron self-absorption and external free-free absorption. Pressure and density gradients in the jets and in surrounding ambient medium are shown to be a primary factor determining the observed properties of ultracompact jets. We discuss possible applications of opacity effects to studying the conditions existing in central regions of active galactic nuclei.

Key words: galaxies: jets – quasars: general – quasars: individual: Cygnus A, 3C 309.1, 3C 345

1. Introduction

Extragalactic jets are believed to be formed in the vicinity of an accretion disk around a supermassive black hole in the center of active galactic nuclei (AGN). Pressure and density gradients, as well as a toroidally shaped magnetic field produced by the rotation of the disk, may collimate the outflowing material into two bipolar streams, and accelerate it up to relativistic speeds (see reviews by Begelman, Blandford, & Rees, 1984; Begelman 1995). Physical conditions in the immediate proximity of an accretion disk determine many aspects of jet evolution at larger spatial scales. The extent of this *ultracompact* fraction of the jet is estimated to be $\sim 0.1 - 10$ pc. Roland et al. (1994) model it as a turbulent region of $\lesssim 1$ pc in size. Marscher & Gear (1985) estimate the projected size of ultracompact jet to be $\sim 0.3h^{-1}$ pc, based on VLBI observations of a radio flare in 3C 273. Königl (1981) and Zensus, Cohen, & Unwin (1995) regard an unresolved core as an ultracompact jet.

In images obtained with Very Long Baseline Interferometry (VLBI), the core is usually identified with the most

compact (often unresolved) feature exhibiting a substantial flux and flat spectrum across the radio band. At any given frequency, the core is believed to be located in the region of the jet where the optical depth is $\tau = 1$. The core absolute position, r_{core} , should therefore depend on the observing frequency, ν_{obs} . Königl (1981) gives $r_{\text{core}} \propto (\nu_{\text{obs}})^{-1/k_r}$. The power index k_r depends on the shape of electron energy spectrum and on the magnetic field and particle density distributions in the ultracompact jet. Observed offsets of the core position at different frequencies have been reported for several sources including 1038+528 A (Marcaide & Shapiro 1984), 4C 39.25 (Guirado et al. 1995), 3C 395 (Lara et al. 1996), and 3C 309.1 (Aaron 1996). Several studies of the core position offset have been undertaken for 3C 345 (Biretta, Moore, & Cohen. 1986; Unwin et al. 1994; Zensus et al. 1995).

In this paper, we discuss synchrotron self-absorption and free-free absorption in the nuclear regions of AGN. We use the frequency dependence of the VLBI core position as a tool for determining the physical conditions of ultracompact jets. In section 2, we describe a model adopted for ultracompact jets, and outline the relations between core shift and physical properties of the jets. Measurements of the shift of VLBI core in radio sources are discussed in section 3. In section 4, the measured core offsets are applied to deriving the magnetic field distribution and physical conditions in the central regions of Cygnus A, 3C 309.1, 3C 345, 3C 395, 4C 39.25, and 1038+528 A.

Throughout the paper, we use a Hubble constant $H_0 = 100 h \text{ km s}^{-1} \text{ Mpc}^{-1}$ and deceleration parameter $q_0 = 0.5$. Unless defined otherwise, all quantities are in the *cgs* units, except for distances which are given in parsecs.

2. Ultracompact jets

A region of significant particle acceleration is assumed to exist at the very center of an AGN. The accelerated particles are confined by an ambient plasma with steep pressure and density gradients along the rotational axis of the central engine. A highly collimated relativistic outflow (jet) can be formed in result. The jet can contain both protons and electron-positron pairs (Sol et al. 1989). Interactions between the jet and the ambient medium are usually ig-

nored, and the jet itself is assumed to have no transverse velocity gradient. The jet hydrodynamics is then given by a stationary adiabatic flow satisfying Bernoulli's equation $(\mathbf{v} \cdot \nabla)\gamma_j p^{1/4} = 0$ (Daly & Marscher 1988). A nozzle is formed at a distance r_c where the pressure p drops below 4/9 of its initial value, and the flow becomes supersonic, with bulk Lorentz factor $\gamma_j(r_c) = 1.22$. Beyond the nozzle, the flow is accelerated by the conversion of internal relativistic particle energy γ_e to bulk kinetic energy γ_{kin} , so that $\gamma_{\text{kin}} \propto \gamma_e \propto r^\epsilon$ ($\epsilon = \text{const}$). The resulting particle energy distribution $N(\gamma_e)$ can be approximated by a power law: $N(\gamma_e) = N_0 \gamma_e^{-s}$ for $\gamma_{\text{min}}(r) < \gamma_e < \gamma_{\text{max}}(r)$, where s is the particle energy spectral index. The jet radiation is then described by the inhomogeneous synchrotron spectrum with spectral index $\alpha = (1 - s)/2$. Unless otherwise specified, the jet bulk Lorentz factor γ_j , and viewing angle θ are assumed constant. The jet geometry can be approximated by a conical or paraboloidal expansion, with the transverse radius $R = a r^\epsilon$ ($\epsilon \leq 1$), for $r_c \leq r \leq r_{\text{max}}$, where r_{max} can be taken $\sim 100\text{--}1000 r_c$, for most of parsec-scale jets. The jet opening angle $\phi = \arctan(R/r)$ is constant for $\epsilon = 1$. The magnetic field and particle density decrease with r , and can be approximated as: $B = B_1 (r_1/r)^m$ and $N = N_1 (r_1/r)^n$, where B_1 , N_1 are the magnetic field and the electron density at $r_1 = 1$ pc. Königl (1981) shows that the combination $m = 1$, $n = 2$ can be used to describe the observed X-ray and synchrotron emission from the most compact regions of VLBI jets.

2.1. VLBI core and ultracompact jet

In the scheme described above, the protons become subrelativistic in the rest frame of the flow outside a characteristic radius r_0 , and the bulk Lorentz factor freezes at the value $\sim \gamma_j = \gamma(r_0)$. This location in the jet is most likely to be observed as the VLBI core (Marscher 1995). It is also referred to as the ‘‘injection point’’ (at which the relativistic plasma is assumed to be injected into the jet at γ_j) in most of the models dealing with parsec-scale relativistic jets.

At any given frequency, the VLBI core is observed at the location where the optical depth of synchrotron self-absorption is $\tau_s = 1$. For given $N(r)$ and $B(r)$, the corresponding τ_s is (e.g. Rybicki & Lightman 1979):

$$\tau_s(r) = C(\alpha) N_1 \left(\frac{e B_1}{2\pi m_e} \right)^\epsilon \frac{\delta^\epsilon \phi_o}{r^{(\epsilon m + n - 1)} \nu^{\epsilon + 1}}. \quad (1)$$

Here m_e is the electron mass and $\epsilon = 3/2 - \alpha$. The observed jet opening angle $\phi_o = \phi \csc \theta$. $C_2(\alpha)$ is described in Blumenthal & Gould (1970), and $C_2(-0.5) = 8.4 \cdot 10^{10}$. Setting $\tau_s(r)$ to unity gives for the distance from the central engine to the core observed at frequency ν

$$r[\text{pc}] = (B_1^{k_b} F / \nu)^{1/k_r}, \quad (2)$$

with

$$F = (1 + z)^{-1} [6.2 \cdot 10^{18} C_2(\alpha) \delta_j^\epsilon N_1 \phi_o]^{1/(\epsilon + 1)}. \quad (3)$$

From (1), $k_r = ((3 - 2\alpha)m + 2n - 2)/(5 - 2\alpha)$ and $k_b = (3 - 2\alpha)/(5 - 2\alpha)$. For the equipartition value of $k_r = 1$, the choice of $m = 1$, $n = 2$ appears to be the most reasonable. The corresponding k_r in this case does not depend on spectral index, and both $B(r)$ and $N(r)$ decline (taking $m = 2$, for instance, would result in $n = 0.5 + \alpha$, which is unrealistic: $N(r)$ would then remain nearly constant, or even grow, with increasing r).

If the apparent core positions measured at two frequencies ν_1, ν_2 ($\nu_1 < \nu_2$) differ by Δr_{mas} , one can introduce a measure of core position offset

$$\Omega_{r\nu} = 4.85 \cdot 10^{-9} \frac{\Delta r_{\text{mas}} D_L}{(1 + z)^2} \cdot \frac{\nu_1^{1/k_r} \nu_2^{1/k_r}}{\nu_2^{1/k_r} - \nu_1^{1/k_r}}, \quad (4)$$

where D_L is the luminosity distance to the source, and frequencies are given in Hz. $\Omega_{r\nu}$ can be used for assessing the quality of core position measurements. For ideal measurements, $\Omega_{r\nu} = (B_1^{k_b} F)^{1/k_r} \sin \theta = \text{const}$, for all frequency pairs. A dispersion in the values of $\Omega_{r\nu}$ derived from different frequency pairs reflects the inaccuracy of core position data. If k_r has been determined inaccurately, or if it varies along the jet, then $\Omega_{r\nu}$ will exhibit a systematic trend. The variations of k_r can occur when the jet crosses a region with rapidly changing absorption properties (e.g. the broad line region). In this case, $\Omega_{r\nu}$ can be used to estimate the change of k_r . If two values $\Omega_{r\nu 1,2}$ (measured between frequencies ν_1 and ν_2) and $\Omega_{r\nu 2,3}$ (between ν_2 and ν_3) are different, the relation between the corresponding k_r 's is:

$$k_{r2,3} \approx k_{r1,2} [\log(\Omega_{r\nu 1,2}) / \log(\Omega_{r\nu 1,3})]. \quad (5)$$

With a measured $\Omega_{r\nu}$, equation (2) can be applied to determine the magnetic field in the jet at $r = 1$ pc

$$B_1 = (\Omega_{r\nu} / \sin \theta)^{k_r/k_b} F^{-1/k_b}, \quad (6)$$

and the absolute distance of the core from the central engine:

$$r_{\text{core}}(\nu) = \Omega_{r\nu} [\nu^{1/k_r} \sin \theta]^{-1}. \quad (7)$$

Formally, r_{core} refers to the distance between the core and the sonic point, r_c . However, since $r_{\text{core}} \gg r_c$, in most cases, r_{core} can be taken as a fair approximation for the distance to central engine. It should also be stressed that r_{core} in (7) depends only on measured quantities (Δr_{mas} and k_r) and on the jet viewing angle θ that can be determined from observations. Therefore r_{core} can be used as a reliable estimate of core position, or at least of the projected distance from the central engine (if θ is poorly known). From (6) and (7), the magnetic field in the VLBI core observed at frequency ν is given by

$$B_{\text{core}}(\nu) \approx \nu^{m/k_r} \left[\frac{\Omega_{r\nu}}{(1 + z) \sin \theta} \right]^\zeta F^{-1/k_b}, \quad (8)$$

where $\zeta = (k_r/k_b) - m$. For a typical $\alpha = -0.5$, we have $\zeta = 0.5$.

Table 1. Predicted core position shift between 5 and 22 GHz

Name	Type	$\Delta r_{5,22}$ [mas]	L_{syn} [erg s ⁻¹]
3C 273	LPQ	0.78	$2.4 \cdot 10^{43}$
3C 216	HPQ	0.70	$3.1 \cdot 10^{43}$
3C 120	LPQ	0.61	$8.4 \cdot 10^{41}$
4C 39.25	LPQ	0.57	$2.2 \cdot 10^{44}$
3C 345	HPQ	0.37	$1.2 \cdot 10^{44}$
1807+698	BL	0.26	$3.3 \cdot 10^{41}$
BL Lac	BL	0.11	$2.3 \cdot 10^{41}$

2.2. Equipartition regime

We now consider the equipartition between jet particle and magnetic field energy densities, with the magnetic field energy density given by $k_e \Lambda B^2 / \pi$ (Blandford & Königl 1979), where $k_e \lesssim 1$, $\Lambda = \ln(\gamma_{\text{max}}/\gamma_{\text{min}})$. In this case, $k_r = 1$ (with $m = 1$, $n = 2$), and the core position offsets can also be used to determine the total (kinetic + magnetic field) power of the jet

$$L_t \approx 2.03 \cdot 10^{29} [\Omega_{r\nu}(1+z)\phi_o]^{3/2} \frac{\Theta(3+2k_e\Lambda)\gamma_j^2\beta_j}{k_e^{1/2}\delta_j\sin\theta}, \quad (9)$$

where $\Theta = \ln(r_{\text{max}}/r_c)$. The L_t can be further used to derive the magnetic field at 1 pc

$$B_1 \approx 2.92 \cdot 10^{-9} \left[\frac{\Omega_{r\nu}^3(1+z)^3}{k_e\delta_j^2\phi\sin^5\theta} \right]^{1/4}. \quad (10)$$

The magnetic field in the core can be obtained, similarly to B_{core} derived in (8). The equipartition can also be used for predicting the core offset in a source with known synchrotron luminosity L_{syn} . In this case, the expected shift of the core position between two frequencies ν_1 and ν_2 is

$$\Delta r_{\text{mas}} \approx \frac{C_r(1+z)}{D_L\gamma^2\phi_o} \frac{\nu_2 - \nu_1}{\nu_1\nu_2} \left[\frac{L_{\text{syn}}\sin\theta}{\beta(1-\beta\cos\theta)\Theta} \right]^{2/3}, \quad (11)$$

with $C_r = 4.56 \cdot 10^{-12}$, and assuming $k_e = 1$. Table 1 contains first order predictions of the core shift between 5 and 22 GHz, for several prominent radio sources.

The synchrotron luminosities in Table 1 are calculated from a database compiled by Ghisellini et al. (1992), using the model of Blandford & Königl (1979) with $\gamma_{\text{max}}/\gamma_{\text{min}} = 100$, $r_{\text{max}}/r_c = 100$. The jet opening angle $\phi = 0.5^\circ$ was used for all sources. The synchrotron self-Compton Doppler factors from the database are used for estimating the jet viewing angles and Lorentz factors, assuming the minimum jet kinetic power condition $\gamma_{\text{min}} = 1/\sin\theta$. This gives lower limits for synchrotron luminosities, and upper limits for the shifts. One can see, from Table 1, that the core shifts may be noticeably large, and can be measured from VLBI data.

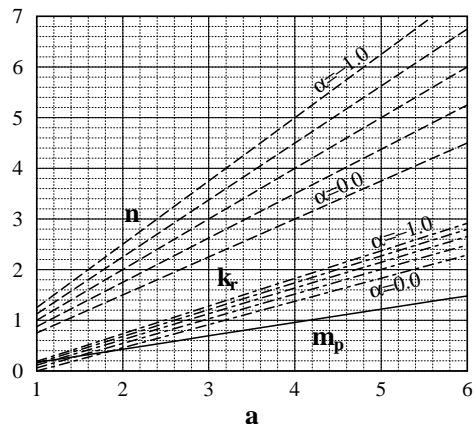


Fig. 1. Physical conditions in the jet in the presence of strong pressure gradients. Power index a describes the pressure gradient ($p \propto r^{-a}$) along the jet axis. The corresponding magnetic field and particle density gradients have power indices m_p (for $m = 1$) and n , respectively. The n and k_r are given for different values of synchrotron spectral index α .

2.3. External pressure gradients

In the vicinity of an accretion disk, physical conditions in the jet become sensitive to the gradients of the pressure $p \propto r^{-a}$ of the ambient medium. Since $\gamma_j p^{1/4} = \text{const}$, to satisfy Bernoulli's equation, the jet Lorentz factor and opening angle vary. Consequently, the corresponding gradients in $B(r)$ and $N(r)$ should also change along the jet in this region (Georganopoulos & Marscher 1996). The dependences of magnetic field and particle density distributions on pressure gradients are shown in Fig. 1. If k_r and spectral index α are measured, one can find, from Fig. 1, the particle density and magnetic field distribution satisfying the conditions of stationary adiabatic flow. The magnetic field at $r \gg r_c$ is $\propto r^{-m_p}$, $m_p = m a / 4$. The particle density distribution can be approximated by $n = a(3 - 2\alpha)/4$.

If the jet is confined by gaseous clouds supported by thermal pressure from the central source and the stellar population with star density ρ_s , the ambient medium density can be modelled by an exponential decrease $p(r) = p_0 \exp(-r^2/d^2)$, with the characteristic size of the cloud system $d = (3kT/\pi G\rho_s m_p)^{0.5}$ (Blandford & Rees 1974). Here m_p is the proton mass, and T is the ambient plasma temperature. Such a distribution reflects the likely conditions in the broad line region (BLR) surrounding the nucleus of an AGN. The jet properties in this case are shown in Fig. 2, for $d = 400r_c$, $a(r_c) = 4$, and $m = 2$. The parameters are chosen so as to approach the equipartition at $r \approx 3d$. The jet opacity to synchrotron self-absorption increases significantly in the region of steepest pressure gradients. This implies that confinement effects may influence the observed frequency dependence of the VLBI core posi-

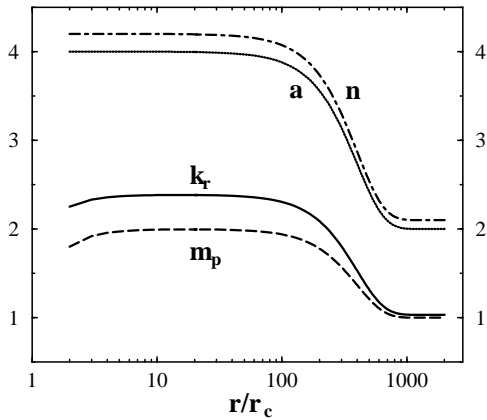


Fig. 2. Change of physical conditions along the jet axis, r . The pressure gradient a corresponds to gaseous clouds supported by thermal pressure and maintaining a mass distribution with spherically symmetrical gravitational potential. The cloud region extends up to $400r_c$ (r_c refers to the distance at which the jet becomes supersonic). The equipartition regime is approached at the outer boundary of the cloud region, with $m_p = 1$, $n = 2$, $k_r = 1$. Significant deviations from the equipartition are seen on smaller scales, resulting in stronger self-absorption in the inner parts of the jet ($k_r \leq 2.5$).

tion in some radio sources. If ρ_s and T are known, the core position measurements can be used for estimating the size of nuclear cloud system.

2.4. Free-free absorption

Foreground free-free absorption in a hydrogen plasma is expected to affect the VLBI-scale radio emission propagating through a dense nuclear environment. The existence of absorbing, circumnuclear plasma has been suggested in 3C 84 (Vermeulen et al. 1994; Walker et al. 1994), Cen A (Jones et al. 1996), and Cyg A (Krichbaum et al. 1997). In all three sources, only the counter-jet emission is believed to be absorbed. One can also expect to find absorption in the jet-side emission, if the jet viewing angle is relatively large, and the absorbing medium extends sufficiently high above the accretion disk plane. One possibility would be the broad line region formed by hydrogen plasma clouds entrained from the disk (Cassidy & Raine 1993). The optical depth of free-free absorption is given by (e.g. Levinson et al. 1995)

$$\tau_{\text{ff}}(r) = 5 \cdot 10^{16} T^{-1.5} \nu^{-2} \bar{g} n_e(r) n_i(r) l_{\text{pc}}, \quad (12)$$

where l_{pc} is the size of absorbing region. Assuming a pure hydrogen plasma with uniform density, we can take $n_e \approx n_i$. The hydrogenic free-free Gaunt factor, \bar{g} , can be evaluated numerically (Hummer 1988). An analytical long-wave approximation of \bar{g} given by Scheuer (1960) can also be used.

The typical sizes of BLR inferred from reverberation mapping and modelling the optical broad line emission of AGN vary between 0.01 and 1 pc (e.g. Kaspi et al. 1996; Baldwin et al. 1996). The corresponding densities of hydrogen plasma are $n_H \sim 10^8 - 10^{12} \text{ cm}^{-3}$. The disk-wind model (Cassidy & Raine 1993) predicts the BLR sizes of up to ~ 20 pc, with n_H between 10^6 and 10^{12} cm^{-3} . There is evidence that weaker emission lines may originate from a very extended ($r \leq 400$ pc) thermal component with densities $n_H \sim 10^2 - 10^8 \text{ cm}^{-3}$ and electron temperatures $T_e \sim 10^4 - 10^6$ K (Ferguson et al. 1997). Most of these plasmas can alter significantly the GHz-range emission from VLBI jets (for instance, $\tau_{\text{ff}} = 250$ at 10 GHz, for $n_e = 10^6 \text{ cm}^{-3}$, $T = 10^4$ K, $l_{\text{pc}} = 0.1$). Udomprasert et al. (1997) report very high rotation measures, $RM \approx 40\,000 \text{ rad m}^{-2}$ in the VLBI core of the quasar OQ 172, which further supports the presence of high-density thermal medium around the ultracompact jets.

For a spherical distribution of BLR clouds, we can take $n_e(r) \propto \epsilon n_0 r^{-n}$ (ϵ is the volume filling factor of the cloud distribution). Then, from (12), $\tau_{\text{ff}} \propto r^{-2n+1}$. A crude estimate $n \approx 3$ can be adopted (remembering that n refers essentially to plasma density variations along the jet axis). Then $r_{\text{core}} \propto \nu^{-2.5}$, and the corresponding core shift is roughly 10 times smaller than that due to synchrotron self-absorption at typical VLBI observing frequencies.

3. Measuring the core position offsets

High-precision measurements of radio source absolute positions which are required for alignment of VLBI images at different frequencies are not readily available in most cases. Extensive absolute astrometry (see Fomalont 1995) observations are necessary, in order to establish a reliable link between VLBI data at different frequencies. In quasi-simultaneous multifrequency observations, the phase-referencing technique (Beasley & Conway 1995) can be sufficient for the purpose of image alignment. If neither of the abovementioned techniques is available, the frequency dependent shift of the core position can be deduced from comparison of observations made at close epochs, assuming that the moving features observed in parsec-scale jets are optically thin and therefore should have their positions unchanged. In this case, the offsets between the component locations measured at different frequencies will reflect the frequency dependent shift of the position of the source core.

3.1. Core shift in 3C 345

An extensive long-term VLBI monitoring database is available for 3C 345 (Zensus et al. 1995, 1997; Lobanov 1996). In the data for 3C 345, there are three close pairs of VLBI observations: (1989.24 at 22.2 GHz)–(1989.26 at 10.6 GHz), (1992.44 at 22.2 GHz)–(1992.45 at 5 GHz), (1993.69 at 5 GHz)–(1993.72 at 22.2 GHz). In these pairs, the separations between the observations in these pairs do not exceed 10 days. We also use two other close pairs with separations of 51 days: (1992.71 at 8.4 GHz)–(1992.86 at 22.2 GHz),

Table 2. Average offsets of the core position in 3C 345

	1	2	3	4	5
Frequency pair	Δr	$b_{\Delta r}$	$\Delta\phi$	Δr_{proj}	
	[mas]		[deg]	[pc]	
5.0– 8.4 GHz	0.05 ± 0.03	5%	-70.8 ± 4.1	0.1	
10.6–22.2 GHz	0.17 ± 0.05	20%	-73.5 ± 2.0	0.6	
8.4–22.2 GHz	0.21 ± 0.06	20%	-71.4 ± 1.4	0.8	
5.0–22.2 GHz	0.33 ± 0.10	28%	-77.1 ± 2.6	1.2	

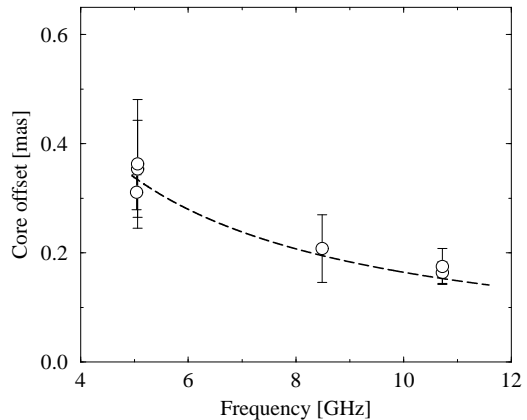
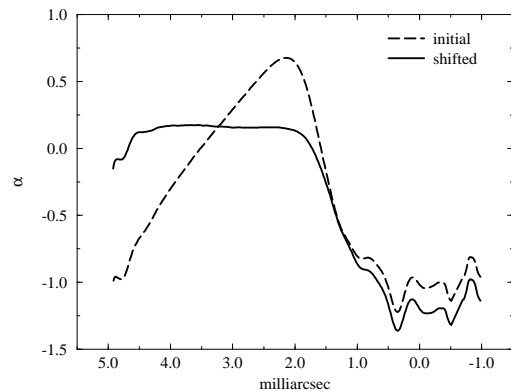
Notes: 2 – offset radius in mas; 3 – corresponding fraction of restoring beam; 4 – position angle of the offset direction; 5 – projected linear distance corresponding to the offset.

and 70 days: (1993.69 at 5 GHz)–(1993.88 at 8.4 GHz). We measure the offsets in the closest and brightest components which have most reliably measured positions. For the pairs with 51 and 70 days separation, the positions of jet components have been corrected for the proper motions measured from the polynomial fits to the components trajectories (Lobanov 1996).

The average angular offsets are compared in Table 2 with the restoring beam sizes of spectral index maps made from the corresponding frequency pairs. The direction of the core shift (-75°) is similar to the position angle of the innermost part of the jet observed at 43 GHz (Krichbaum & Witzel 1992). Between 5 and 8.4 GHz, the position shift cannot be measured reliably because of the insufficient resolution and errors due to the proper motion corrections. The measured shift constitutes only about 5% of the restoring beam. With increasing frequency separation, the position shift becomes a prominent fraction of beamsize (up to 27% for spectral index maps between 5 and 22.2 GHz). Fig. 3 shows the measured offsets with respect to the reference frequency (22.2 GHz). The 5–8.4 GHz measurements are not included. The dashed line in Fig. 3 represents the best fit: $r \propto \nu^{(-1.04 \pm 0.16)}$.

3.2. Effect of the reference point offset on spectral imaging

Whenever an offset constitutes a significant fraction of restoring beam, it can influence substantially the derived spectral properties. An example of this effect is shown in Fig. 4. The 5–22 GHz spectral index profiles shown in Fig. 4 are measured along the jet ridge line in the nuclear region of 3C 345. The core extends from +2 to +5 mas. The profile obtained by aligning the images on their respective core positions shows a strong gradient, with optically thin spectral index across a significant fraction of the core. Applying the measured core position offset between 5 and 22.2 GHz levels the spectral index across the entire core, with $\alpha_{\text{core}} \approx 0.2$. Similar corrections applied to several other spectral index maps of 3C 345 have resulted in decreased peak values, and

**Fig. 3.** Frequency dependent shift of the core position in 3C 345. Dashed line corresponds to $r \propto \nu^{-1.04}$. Reference frequency is 22.2 GHz.**Fig. 4.** Spectral index profiles taken in the nuclear region of 3C 345 (5–22.2 GHz, September 93). Dashed line is the spectral index profile obtained by aligning both images by their respective core positions. Solid line is the profile obtained after applying the measured position offset of the core.

smoother spectral index distributions across the nuclear region.

4. Properties of ultracompact jets

To illustrate the implications of frequency dependence of VLBI core position, we calculate physical properties of ultracompact jets in 3C 345 and 5 other AGN with reported core position offsets. Table 3 summarizes the model parameters (panel A), and gives the measured and derived quantities (panel B). For all sources, we assume $m = 1$, $n = 2$, and use crude estimates $\gamma_{\text{max}}/\gamma_{\text{min}} = 100$, and $r_{\text{max}}/r_c = 100$ (since only the logarithms of these ratios affect the calculated luminosities). The value of N_1 is determined in

Table 3. Model and derived parameters of ultracompact jets

A. MODEL PARAMETERS							
Name	z	γ_j	θ_j [deg]	ϕ_j [deg]	α_j	N_1 [cm ⁻³]	Refs.
Cyg A	0.0562	5.0	80.0	7.0	-0.5	8000	1,2
3C309.1	0.905	5.0	20.0	2.0	-0.6	17000 [†]	3
3C345	0.594	5.6	7.6	2.4	-0.6	1300 [†]	4,5
3C395	0.635	7.1	8.7	0.5	-0.6	1800 [†]	6
4C39.25	0.699	11.0	30.0	4.0	-0.5	1000 [†]	7
1038+528A	0.678	4.0	20.0	5.0	-0.6	1900 [†]	8

References: 1 – Krichbaum et al. 1997; 2 – Carilli & Barthel 1996; 3 – Kus 1993; 4 – Zensus et al. 1997; 5 – Lobanov 1996; 6 – Lara et al. 1994; 7 – Alberdi et al. 1993; 8 – Marcaide et al. 1994.

B. MEASURED AND DERIVED PARAMETERS [§]								
Name	ν_1/ν_2 [GHz]	$\Omega_{r\nu}$ [pc GHz ⁻¹]	B_1 [G]	B_{core}^\dagger [G]	r_{core}^\dagger [pc]	L_{tot} [10 ⁴⁶ erg s ⁻¹]	L_{syn} [10 ⁴⁶ erg s ⁻¹]	$T_{\text{b max}}$ [10 ¹¹ K]
Cyg A	22/43	2.1 ± 0.4	0.07 ± 0.01	0.7 ± 0.3	0.10 ± 0.02	0.55 ± 0.05	0.07 ± 0.01	1.0
3C309.1	1.5/2.3	16.3 ± 7.2	1.2 ± 0.4	0.6 ± 0.4	2.1 ± 0.9	5.8 ± 1.7	0.71 ± 0.21	7.2
	1.6/2.3	15.4 ± 8.8	1.1 ± 0.5	0.5 ± 0.4	2.0 ± 1.2	5.3 ± 2.3	0.66 ± 0.28	7.2
	2.3/5.0	7.2 ± 3.6	0.4 ± 0.1	0.4 ± 0.3	0.9 ± 0.5	1.7 ± 0.6	0.21 ± 0.07	6.5
	5.0/8.4	< 5.2	< 0.2	< 0.3	< 0.7	< 1.0	< 0.1	< 6.3
	8.4/15.1	< 8.0	< 0.4	< 0.4	< 1.0	< 2.0	< 0.2	< 6.6
3C345	10.6/22.2	13.1 ± 3.8	1.9 ± 0.3	0.4 ± 0.2	4.4 ± 1.3	19.8 ± 3.2	2.4 ± 0.4	25.8
	8.4/22.2	10.8 ± 3.1	1.4 ± 0.6	0.4 ± 0.2	3.7 ± 1.0	14.7 ± 2.2	1.8 ± 0.3	25.1
	5.0/22.2	8.1 ± 2.4	0.9 ± 0.2	0.3 ± 0.2	2.8 ± 0.8	9.6 ± 1.6	1.2 ± 0.2	24.2
3C395	2.3/8.4	7.4 ± 2.4	1.4 ± 0.6	0.7 ± 0.4	2.2 ± 0.7	1.0 ± 0.2	0.12 ± 0.02	22.2
4C39.25	2.3/8.4	6.3 ± 1.3	0.6 ± 0.2	1.0 ± 0.4	0.6 ± 0.1	18.2 ± 1.6	2.2 ± 0.2	2.4
1038+528A	2.3/8.4	6.3 ± 1.2	0.4 ± 0.1	0.5 ± 0.2	0.8 ± 0.2	2.6 ± 0.2	0.32 ± 0.03	7.4
	8.4/15.1	< 1.5	< 0.13	< 0.3	< 0.2	< 0.3	< 0.04	< 6.2

Notes: [§] – only the errors due to uncertainties of the core offset measurements are considered; [†] – derived by equating B_1 to its equipartition value; [‡] – B_{core} and r_{core} are given for $\nu_{\text{obs}} = 22.2$ GHz.

most cases, by setting B_1 to its equipartition value given by (10). Synchrotron luminosity, L_{syn} , and maximum brightness temperature, $T_{\text{b max}}$, are calculated using the model of Blandford and Königl (1979). For the purpose of comparison between different sources, the offset measures, $\Omega_{r\nu}$ are given, rather than the angular offsets cited in the original publications.

4.1. Cygnus A

We adopt the component identification made by Krichbaum et al. (1997), and use their position measurements to derive the offset of the core in Cygnus A between 22.2 and 43.2 GHz (observation epochs 1992.44 and 1990.40, respectively). Krichbaum et al. (1997) give Gaussian model fits describing the compact structure of the source. We use these models to calculate the shifts of the total of four

features situated both in the jet (components J3, J4) and counter-jet (components C1, C2). The two closest jet-side components, J1 and J2, are blended together in the model at 22 GHz. The averaged shifts are: $\Delta r_j = 74 \mu\text{s}$ for J3 and J4, and $\Delta r_{\text{cj}} = -54 \mu\text{s}$ for C1 and C2. The negative sign for the shift on the counter-jet side indicates that the component separations from the core are shorter at 43.2 GHz. This fact further supports the identification, as well as frequency dependence, of the core location in Cygnus A. We then estimate that the shift of the core position amounts to $64 \pm 12 \mu\text{s}$, and use this value for calculating the physical properties of the jet.

The estimated $B_1 = 0.07$ G is consistent with the field strength ($B_{1\text{pc}} \approx 0.06$ G, for $\phi_j = 7.0^\circ$) in a Poynting flux jet (Lovell & Romanova 1996) driven by a $3 \cdot 10^8 M_\odot$ black hole. Carilli & Barthel (1996, CR96 hereafter) use the unresolved core flux density of Cygnus A at 43 GHz,

and apply the minimum energy equation, to arrive at $B_m = 0.16$ G in a nuclear region of 0.15 mas (0.11 pc) in size. We have $r_{43\text{ GHz}} \approx 0.05$ pc, for the distance from the jet origin to the core observed at 43 GHz. With these values, $B_1 = 0.11B_m \tan \phi_j / r_{43\text{ GHz}} \approx 0.06$ G.

The total jet power, L_{tot} , can be related to the luminosity of extended radio lobe, L_R : $L_{\text{tot}} = L_R / \eta$ (CR96), with $\eta = 0.01\text{--}0.1$ (Leahy 1991) describing the efficiency of converting bulk kinetic energy into radio luminosity. In Cygnus A, the lobe radio luminosity $L_R = 4.4 \cdot 10^{44}$ erg s $^{-1}$ (CR96), which results in $\eta = 0.08$, for our derived L_{tot} .

The predicted location, $r_{\text{c.e.}}$, of the central engine in Cygnus A is offset by about 0.14 mas from the core. Comparison between the 22 GHz flux densities of two bright features (J2 on the jet side, and C1 on the counter-jet side) evenly separated from $r_{\text{c.e.}}$ gives 2.2 ± 0.3 for the jet-to-counter-jet ratio (this figure should be viewed as an upper limit, if a foreground absorbing medium is present). The calculated ratio results in $\theta_j = 80.6 \pm 1.2$ for the adopted $\gamma_j = 5$. Conversely, for $\theta = 80.0$ used in the model, the corresponding $\beta_j = 0.92^{+0.08}_{-0.11}$.

4.2. 3C 309.1

We use the position measurements of Aaron (1996 and priv. comm.), and adopt the jet geometry as modelled by Kus (1993). Only upper limits are available for the core offset at frequencies higher than 5 GHz, as the separation between the core and closest optically thin feature remains constant. The derived $\Omega_{r\nu}$ decrease substantially towards higher frequencies. We take it as evidence for larger k_r due to increasing opacity at shorter distances from the jet origin. Between 1.5 and 2.3 GHz, k_r is likely to be close to unity, so we take the corresponding derived quantities as best estimates of physical conditions in the jet. The estimated $N_1 = 17000$ is larger than in the other objects listed in Table 3, possibly implying a stronger pressure confinement in 3C 309.1. The latter can be reconciled with the results from optical spectroscopy (Forbes et al. 1990) suggesting that 3C 309.1 may have a massive ($\dot{M} \geq 1000 M_\odot \text{yr}^{-1}$) cooling flow within a radius of $11.5 h^{-1}$ kpc.

The variations of k_r necessary to account for the difference in measured $\Omega_{r\nu}$ are compared in Fig. 5 with changes due to the pressure gradients described in section 2.3. Here we assign $r_{\text{core}}(1.5\text{ GHz}) = 1200 r_c$, treat upper limits of $\Omega_{r\nu}$ as measured points, and use the same model parameters as in Fig. 2. The behavior of jet opacity displayed in Fig. 5 is in agreement with the measurements of Aaron et al. (1997), who report a moderately high rotation measure $RM_{\text{core}} \sim -1600$ with strong gradients across a nuclear region of $\sim 3 h^{-1}$ pc in size. It should be stressed however that the model shown in Fig 5 is used for purely illustrative purposes, and we do not attempt to make quantitative conclusions or rule out other explanations for the observed core offsets in 3C 309.1. For instance, external free-free absorption in the BLR clouds may result in similar changes of k_r .

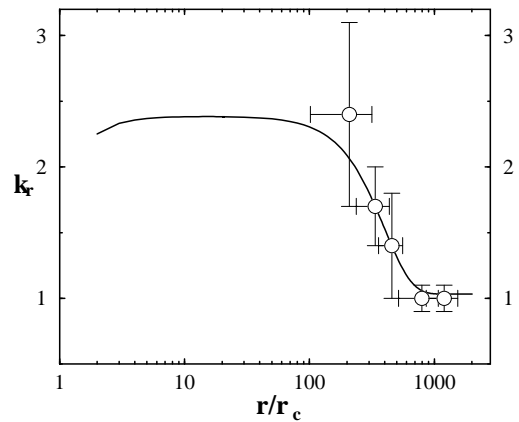


Fig. 5. Opacity in the jet of 3C 309.1. Circles are the measured values of k_r in 3C 309.1 at different frequencies; solid line shows changes of k_r due to pressure gradients described in section 2.3. The model parameters are the same as in Fig. 2.

4.3. 3C 345

Properties of the ultracompact jet in 3C 345 have been discussed recently in several papers, based on X-ray (Unwin et al. 1994, 1997), VLBI (Zensus et al. 1995), and multi-frequency observations of the source (Bregman et al. 1986; Webb et al. 1994; Stevens et al. 1996). We adopt a spectral index $\alpha_j = -0.6$ (Unwin et al. 1994), and derive the geometric parameters for our model from the statistical properties of superluminal features embedded in the extended jet (Zensus et al. 1995; Lobanov 1996).

To obtain a plausible estimate of δ_j , one can assume that the jet carries the least kinetic power, so that $\gamma_j = (1 + \beta_{\text{app}}^2)^{0.5}$ (the assumption is valid only if the observed speeds are those of bulk motions in the jet). Under this assumption, the variations of viewing angle are derived for the jet components in the immediate vicinity of the core (Lobanov 1996); and we estimate $\gamma_j \approx 5.6$ and $\theta_j \approx 7.6^\circ$ for the Lorentz factor and viewing angle of the ultracompact jet in 3C 345. These values are close to the fitted values from the synchrotron self-Compton (SSC) models applied to 3C 345 (Unwin et al. 1994; Webb et al. 1994).

The jet opening angle, $\phi_j \approx 2.4^\circ$, is calculated from measuring the jet size within 1 mas distance from the core. The particle density $N_1 = 1300 \text{ cm}^{-3}$ is almost 20 times smaller than the value given in Unwin et al. (1994) for an SSC model of the VLBI core. Zensus et al. (1995) have indicated that the SSC value of N_1 might be roughly 10 times smaller, to accommodate the magnetic field and particle density found in the jet superluminal features. The latter prediction is consistent with our estimate of N_1 within a factor of 2.

The calculated offset measures in 3C 345 given in Table 3 decrease at lower frequencies. The corresponding k_r must decrease by about 20%, between 5 and 11 GHz (which

Table 4. Derived parameters of the ultracompact jet

ν [GHz]	B_{core} [G]	Δr_{pc}	Δr_{mas}
5.0	0.09 ± 0.05	16.3 ± 4.6	0.57 ± 0.16
8.4	0.15 ± 0.08	9.7 ± 2.8	0.34 ± 0.10
10.6	0.18 ± 0.10	7.7 ± 2.2	0.27 ± 0.08
22.2	0.38 ± 0.21	3.7 ± 1.0	0.13 ± 0.04

Notes: the angular offsets are given for a jet with $\theta = 7.6^\circ$.

is within the errors of the fit given in Fig. 3). Assuming that $k_r(5 \text{ GHz}) = 1$, the decrease in $\Omega_{r\nu}$ corresponds to $k_r(11 \text{ GHz}) = 0.81 \pm 0.14$. This implies that the optical depth in the jet also becomes smaller at higher frequencies — a situation that does not have a simple explanation in the frameworks of both synchrotron self-absorption and external free-free absorption. With this argument in mind, and also considering the magnitude of errors in the derived offset measures, it appears more likely that the decrease of $\Omega_{r\nu}$ results from blending effects due to the limited resolution. With decreased angular resolution at lower frequencies, the blending between the core and a nearest jet feature (remaining unidentified in the VLBI maps) should become progressively stronger, resulting in a systematic trend in $\Omega_{r\nu}$. However, we cannot entirely exclude an explanation involving peculiar physical conditions in the source. We therefore take the average $\Omega_{r\nu} = 10.7 \pm 5.4$ as the reference value for 3C 345.

The corresponding average characteristic magnetic field, $B_1 = 1.4 \pm 0.7 \text{ G}$, is lower than most of the values obtained by Webb et al. (1994), but can be reconciled with the results from Unwin et al. (1994), considering the difference of the adopted particle densities.

The average total power of the jet is $L_t \approx (1.5 \pm 0.4) \cdot 10^{47} \text{ erg s}^{-1}$, and we find $L_{\text{syn}} \approx (1.8 \pm 0.5) \cdot 10^{46} \text{ erg s}^{-1}$. With the derived magnetic field, the maximum brightness temperature is $T_{\text{b max}} \approx 2.5 \cdot 10^{12} \text{ K}$. The obtained value is consistent with the 10^{12} K inverse Compton limit, similarly to the mean values of the maximum brightness temperature in a sample of superluminal sources (Vermeulen & Cohen 1994). Arguments based on the hypothesis of equipartition between relativistic particle and magnetic energy density ($\varepsilon_p/\varepsilon_B \sim 1$) predict a lower value of maximum brightness temperature $T_{\text{b eq}} \approx 4.5 \cdot 10^{11} \text{ K}$, Readhead 1994). The relativistic particle energy density, $\varepsilon_p \propto T_{\text{b}}^{4.5}$, and the energy density in the magnetic field, $\varepsilon_B = B^2/8\pi \propto T_{\text{b}}^{-4}$. This gives $\varepsilon_p/\varepsilon_B \approx (T_{\text{b max}}/T_{\text{b eq}})^{8.5} \approx 2 \cdot 10^6$ for the ultracompact jet, and therefore the jet must lose its energy through X-ray emission due to inverse Compton scattering. Unwin et al. (1994) argue that physical conditions in the extended jet may as well deviate significantly from the equipartition. According to Unwin et al. (1994), $\varepsilon_p/\varepsilon_B \sim 10^2 - 10^4$ at $r \sim 10-100 \text{ pc}$, which can be a natural consequence of evolution and radiation losses

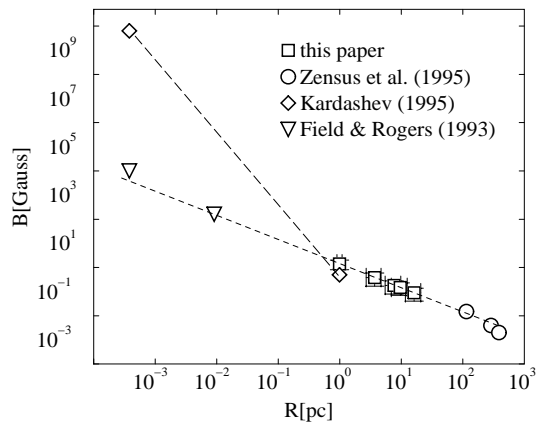


Fig. 6. Magnetic field distribution in 3C 345. Squares show the magnetic field in the compact jet derived from the frequency dependent shift of the core. Circles are the homogeneous synchrotron model estimates of magnetic field in the extended jet components (Zensus et al. 1995). Triangles show the characteristic magnetic field values from a model of magnetized accretion disk (Field and Rogers, 1993). Diamonds are the theoretical estimates from Kardashev’s (1995) model for the dipole magnetic field around a supermassive rotating black hole.

in a plasma with original $\varepsilon_p/\varepsilon_B \sim 10^6$.

4.4. Magnetic field in the jet of 3C 345

Table 4 summarizes the derived positions and magnetic fields in the VLBI core of 3C 345 at different frequencies. According to the derived positions, the location of the core observed at 22 GHz should be about 4 pc away from the jet origin. The angular offsets are all smaller than the VLBI beam size at corresponding frequency; therefore, the central engine is likely to be blended with the VLBI core even if the opacity is low enough for the emission from the innermost regions of the jet to be observed. Under such circumstances, evidence for emission from the inner jet can only be found in the spectral index or turnover frequency maps (Lobanov et al. 1997).

In Fig. 6, the derived magnetic field is compared with the values obtained from synchrotron emission calculations for the extended jet (Zensus et al. 1995), as well as with model predictions for the central engine in 3C 345. The theoretical values of magnetic field in the close vicinity of central engine are calculated from a model of thin, magnetically driven accretion disk (Field and Rogers 1993), and from a model of supermassive black hole surrounded by a strong magnetic field (Kardashev 1995). The accretion disk model predicts $B \approx 10^4$ at $r \approx R_g$, and $B \approx 160 \text{ G}$ at $r \approx 24R_g$ ($R_g = 2GM_{\text{bh}}/c^2$ is the Schwarzschild radius of the central black hole). The mass of central black hole can be related to B_1 , so that $M_{\text{bh}} \approx 2.7 \cdot 10^9 B_1 M_\odot$; and in 3C345: $M_{\text{bh}} \approx 4 \cdot 10^9 M_\odot$. Kardashev (1995) suggests that a strong dipole magnetic field may exist in the

vicinity of a supermassive black hole. The maximum field strength can be estimated from the equilibrium relations $M_{\text{bh}} \sim M_{\text{d}} \sim M_{\text{B}}$, where M_{bh} , M_{d} , M_{B} are masses of black hole, its disk, and its magnetic field respectively. Then $B_{\text{max}} = c^4 G^{-1.5} M_{\text{bh}}^{-1} = 2.4 \cdot 10^{19} (M_{\text{bh}}/M_{\odot})^{-1}$. This gives for 3C 345: $B_{\text{max}} \approx 6.3 \cdot 10^9$ G. For a dipole magnetic field, one obtains $B \propto r^{-3}$, so that $B \approx 0.8$ G at 1 pc, slightly lower than our estimate in Table 3. To match the derived B_1 , the mass of central black hole in Kardashev's model must be $M_{\text{bh}} = (cB^{1/2}r^{3/2})/(2\sqrt{2}G^{3/4}) \approx 7 \cdot 10^9 B^{1/2}r^{3/2}M_{\odot} \approx 8.3 \cdot 10^9 M_{\odot}$.

4.5. 3C 395 and 4C 39.25

The core offsets are known from geodetic VLBI measurements between 2.3 and 8.4 GHz (Lara et al. 1996; Guirado et al. 1995). We use the models derived for the parsec-scale jets in these sources (Lara et al. 1994; Alberdi et al. 1993), and adopt the equipartition values of N_1 . The resulting $\Omega_{r\nu}$ are similar to the 2.3–5 GHz offset measure in 3C 309.1. Other derived parameters are also comparable to their counterparts in 3C 345 and 3C 309.1. The derived synchrotron luminosity of 4C 39.25 is quite high, compared to $L_{\text{syn}}(10\text{--}90\text{ GHz}) = 5.5 \cdot 10^{44}$ erg s $^{-1}$ given in Bloom & Marscher (1991), even taking into account the spectral limits.

Recent observations of 4C 39.25 at 22.2 and 43.2 GHz (Alberdi et al. 1997) indicate no detectable position shift in the source. From the measured $\Omega_{r\nu}$ between 2.3 and 8.4 GHz, the expected shift between 22.2 and 43.2 GHz is less than 0.05 mas. The latter value is below the image resolution at both frequencies (≈ 0.3 and ≈ 0.17 mas).

4.6. 1038+528 A

Marcaide & Shapiro (1984) reported a 0.7 mas shift between 2.3 and 8.4 GHz in 1038+528 A. Subsequently, Marcaide et al. (1985) derived $0.5 < k_{\text{r}} < 1.4$, based on VLBI data at 1.4, 2.3, 8.4, and 10.6 GHz. Marcaide, Elósegui & Shapiro (1994) applied a relativistic shock model by Gomez et al. (1993) to explain the observed shift. Rioja & Porcas (1997) have made position measurements at 2.3, 8.4, and 15 GHz, and argued that at least a fraction of the observed offset can result from limited resolution and blending at lower frequencies. The $\Omega_{r\nu}(2.3\text{--}8.4\text{ GHz})$ calculated from the data of Rioja et al. (1997) is similar to the values obtained for 4C 39.25 and 3C 395 (although the projection effects should be kept in mind, in view of the different viewing angles in these sources). The upper limit given for the offset between 8.4 and 15 GHz corresponds to $k_{\text{r}} \geq 4.4$, making it rather difficult to be explained by synchrotron self-absorption. Even for free-free absorption, it would require very strong density gradients ($n \geq 4$) in the absorbing medium, in order to reproduce the given limit on k_{r} .

5. Opacity in the jets

Assuming that the frequency term in (4) dominates core position offsets, the measured $\Omega_{r\nu}$ can be used for compar-

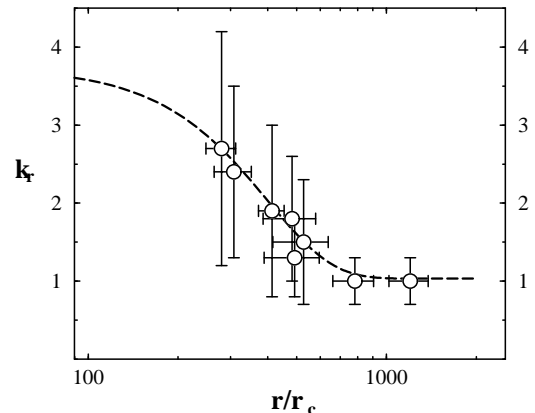


Fig. 7. Relative changes of opacity in the ultracompact jets. Reference point is the 1.5–2.3 GHz offset in 3C 309.1, with $k_{\text{r}} = 1$ and $r = 1200r_{\text{c}}$ assigned to it. For the rest of the data, the k_{r} and r are calculated from the corresponding $\Omega_{r\nu}$ measured in the respective source rest frames. Dashed line is a model similar to that described in section 2.3, but with $a(r_{\text{c}}) = 6$.

ing the relative opacity in different sources. To make such a comparison, the offset measures and observing frequencies must be transformed to the respective source rest frames: $\Omega'_{r\nu} = \Omega_{r\nu} \sin \theta_j (1 + z)$; $\nu' = \nu(1 + z)$. We then postulate that the largest $\Omega'_{r\nu}$ corresponds to $k_{\text{r}} = 1$, $r = 1200r_{\text{c}}$, and use it as a reference point for calculating the k_{r} for the rest of the offset measurements. The results are plotted in Fig. 7. In 3C 395, the calculated k_{r} is very large ($k_{\text{r}} > 17$), suggesting that the jet viewing angle may be greater than the value cited by Lara et al. (1994). The apparent increase of k_{r} at shorter radial distances is consistent with the self-absorption scenario described in section 2.3 (the measured $\Omega'_{r\nu}$ become smaller at higher frequencies at which the opacity is larger). The linear scale in Fig. 7 serves only as an illustration, since the intrinsic properties of the sources (reflected by the $B_1^{k_{\text{b}}} F$ term) may be different. Detailed studies of each individual object are required for establishing a connection between the jet linear scale and opacity properties. A general prediction is that the position offset should be larger in flat-spectrum cores in which $k_{\text{r}} \sim 1$. When k_{r} increases, the offsets are expected to become smaller, and the core spectrum should be inverted.

A reasonably good agreement found in Fig. 7 between the derived and model k_{r} indicates that synchrotron self-absorption may be responsible for the observed properties of optically thick emission from ultracompact jets. One can expect then to find similar physical conditions in the VLBI cores of different sources, if the measurements are done at the same rest frame frequency. To illustrate this, we calculate the magnetic fields and core distances at $\nu' = 22$ GHz, and plot them versus jet synchrotron luminosity (Fig. 8). The derived r_{core} increase, with increasing

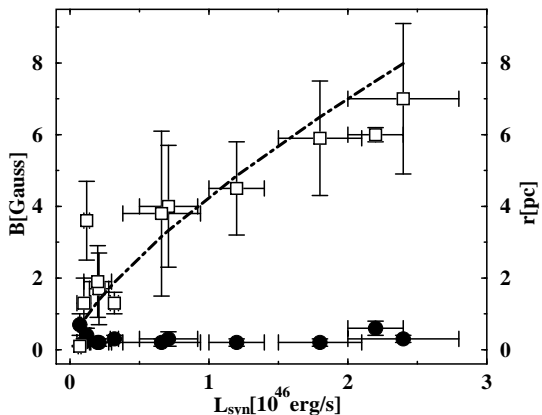


Fig. 8. Magnetic field (filled circles) and distance of the core (squares) with respect to the jet synchrotron luminosities. The data are shown for $\nu' = 22$ GHz. Dot-dashed line is $r_{\text{core}} \propto L_{\text{syn}}^{2/3}$.

L_{syn} , and follow roughly the proportionality $r_{\text{core}} \propto L_{\text{syn}}^{2/3}$ resulting from (7) and (9). The corresponding magnetic field however remains nearly constant, with an average of $B_{\text{core}} = 0.30 \pm 0.08$ [G]. One may expect the values of magnetic field to vary stronger, and exhibit a rather large scatter, if jet emission is affected by external factors such as free-free absorption. The homogeneity of B_{core} seen in Fig. 8 suggests that the jet plasma is a primary factor determining the location and properties of VLBI cores, and that intrinsic physical conditions in the jets must be fairly similar. If this suggestion holds for other sources, the expected magnetic field in VLBI core should be of the order of $B_{\text{core}}(\nu_{\text{obs}}) \approx 0.3 [0.045\nu_{\text{obs}}(1+z)]^{m/k_r}$ [G], for ν_{obs} measured in GHz.

6. Conclusions

The frequency dependent position shift of VLBI cores can be used for studying the most compact regions of extragalactic jets, and obtaining quantitative estimates for physical conditions in the immediate vicinity of central engine. In the absence of high-precision position measurements, a more simplistic approach can be employed, assuming that positions of optically thin features in the jet remain the same at all frequencies. Then, the position offsets of optically thin features can be interpreted as a frequency dependent shift of the self-absorbed core of the jet. In some sources (1038+528 A, 3C 345, Cygnus A), insufficient resolution and blending at lower frequencies may undermine the offset measurements. A way to detect and, to a certain degree, to correct the errors due to the blending can be found in introduction of an offset measure, $\Omega_{r\nu}$, which is supposed to remain constant for the case of ideal measurements and unchanged opacity of the jet. Listed below

are the main results from deriving the offset measures in 6 sources with reported position offsets of VLBI core:

1. The jet luminosity, the maximum brightness temperature, the core magnetic field and location with respect to the jet origin can be determined, from offset measures. For the well studied sources (Cygnus A, 3C 345), the derived values are shown to agree well with values determined by other methods. In Cygnus A, the jet-to-counter-jet ratio determined from the estimated location of the central engine results in a self-consistent source geometry. In 3C 345, the derived maximum brightness temperature indicates that the ultracompact jet is strongly particle-dominated, and must release its energy through inverse Compton scattering. The obtained magnetic field distribution in the ultracompact jet of 3C 345 is in a good agreement with the values derived from inhomogeneous synchrotron models applied to the extended jet components. Based on the derived characteristic magnetic field, it appears more likely that the jet is produced by a thin, magnetized accretion disk, rather than by a single supermassive black hole with a strong dipole magnetic field.

2. External pressure and density gradients typical for the broad line region may change the optical depth along the jet via both synchrotron self-absorption and free-free absorption in an ambient medium. The offset measures derived for different frequency pairs and different objects can be used for studying the opacity effects in ultracompact jets. Changes of jet opacity in 3C 309.1 deduced from the variations of k_r appear to be consistent with a self-absorbed jet propagating through a region with strong density gradients. Similar conclusion can be drawn from the variations of k_r determined for all studied objects, although the agreement with the model may in this case be coincidental (one argument for making such a reservation is that the initial pressure gradients required to fit the data for all sources simultaneously are very high: $N(r) \propto r^{-6}$, at $r \sim r_c$).

3. The distance at which the observed VLBI core is located at a given frequency is scaled with jet luminosity, so that $r_{\text{core}} \propto L_{\text{syn}}^{2/3}$. At the same time the magnetic field in the core appears to be almost unchanged, from one source to another. This can be taken as another evidence for the synchrotron self-absorption to be a primary factor influencing the observed properties of the jet core.

Further, more detailed studies of absorption in ultracompact jets are required for confirming the conclusions stated above, and for constructing better models of individual sources. Nearly simultaneous, multifrequency VLBI data obtained with phase-referencing should be most useful for a reliable determination of the core offsets, and subsequent studies of the most compact regions in active galactic nuclei.

Acknowledgements

We would like to thank S. Aaron, T. Krichbaum, R. Porcas and M. Rioja for fruitful discussions and providing the unpublished data for this study.

References

- Aaron, S.E. 1996, Ph.D. Thesis, Brandeis University
- Aaron, S.E., Wardle, J.F.C, and Roberts, D.H. 1997, *Vistas in Astronomy*, 41, 225
- Alberdi, A., Marcaide, J.M., Marscher, A.P. et al. 1993, *ApJ*, 402, 160
- Alberdi, A., Krichbaum, T.P., Graham, D.A., et al. 1997, *A&A* (in press)
- Baldwin, J.A., Ferland, G.J., Korista, K.T. et al. 1996, *ApJ*, 461, 664
- Beasley, A.J. & Conway J.E. 1995, in *Very Long Baseline Interferometry and the VLBA*, eds. J.A. Zensus, P.J. Diamond, & P.J. Napier (Cambridge, Cambridge University Press), 291
- Begelman, M.C. 1995, in *Publications of the National Academy of Sciences, Vol.92, Quasars and Active Galactic Nuclei: High Resolution Radio Imaging*, eds. M.H. Cohen & K.I. Kellermann (reprint: Charlottesville, NRAO), 11442
- Begelman, M.C., Blandford, R.D., & Rees, M.J. 1984, *Rev. Mod. Phys.*, 56, 255
- Biretta, J.A., Moore, R.L., & Cohen, M.H. 1986, *ApJ*, 308, 93
- Blandford, R.D. & Königl, A. 1979, *ApJ*, 232, 34.
- Blandford, R.D. & Rees, M.J. 1974, *MNRAS*, 169, 395
- Bloom, S.D. & Marscher, A.P. 1991, *ApJ*, 366, 16
- Blumenthal, G.R. and Gould, R.J. 1970, *Rev. Modern Phys.*, 4, 237
- Bregman, J.N., Glassgold, A.E., Huggins, P.J., et al. 1986, *ApJ*, 301, 708
- Carilli, C.L. & Barthel, P.D. 1996, *A&A Rev.*, 7, 1
- Cassidy, I. & Raine, D.J. 1993, *MNRAS*, 260, 385
- Daly, R.A., Marscher, A.P. 1988, *ApJ*, 334, 539
- Ferguson, J.W., Korista, K.T., & Ferland, G.J. 1997, *ApJS*, 110, 287
- Field, G.B. & Rogers, R.D. 1993, *ApJ*, 403, 94
- Fomalont, E. 1995, in *Very Long Baseline Interferometry and the VLBA*, eds. J.A. Zensus, P.J. Diamond, & P.J. Napier (Cambridge, Cambridge University Press), 205
- Georganopoulos, M. & Marscher, A.P. 1996 in “Energy Transport in Radio Galaxies and Quasars”, eds. P.E. Hardee, A.H. Bridle, J.A. Zensus, ASP Conference Series, v.100, 67
- Gomez, J.L., Alberdi, A., & Marcaide, J.M. 1993 *A&A* 274, 55
- Ghisellini, G., Celotti, A., George, I.M., & Fabian, A.C. 1992, *MNRAS*, 258, 776
- Guirado, J.C., Marcaide, J.M., Alberdi, A., et al. 1995, *AJ*, 110, 2586
- Jones, D.L., Tingay, S.J., Murphy, D.W., et al. 1996, *ApJ*, 466, 63
- Hummer, D.G. 1988, *ApJ*, 327, 477
- Kaspi, S., Smith, P.S., Maoz, D., Netzer, H., Januzzi, B.T. 1996, *ApJ*, 471, L75
- Königl, A. 1981, *ApJ*, 243, 700
- Krichbaum, T.P., Alef, W., Witzel, A., Zensus, J.A., Booth, R.S., Greve, A., & Rogers, A.E.E. 1997 *A&A*, in press
- Krichbaum, T.P. & Witzel, A. 1992, in “Variability of Blazars”, eds. E. Valtaoja & M. Valtonen (Cambridge: CUP), p.205
- Kardashev, N.S. 1995, *MNRAS*, 276, 515
- Kus, A.J. 1993, in “Sub-arcsecond Radio Astronomy”, eds. R.J. Davis & R.S. Booth (Cambridge: CUP), p.365
- Lara, L., Alberdi, A., Marcaide, J.M., & Muxlow, T.W.B. 1994, *A&A*, 285, 393
- Lara, L., Marcaide, J.M., Alberdi, A., & Guirado, J.C. 1996, *A&A*, 314, 672
- Leahy, J.P. in “Beams and Jets in Astrophysics”, ed. P.A. Hughes (Cambridge: CUP), p.100
- Levinson, A., Laor, A., & Vermeulen, R.C. 1985, *ApJ*, 448, 589
- Lobanov, A.P. 1996, Ph.D. Thesis (New Mexico Institute of Mining and Technology, Socorro NM)
- Lobanov, A.P., Carrara, E., & Zensus, J.A. 1997, *Vistas in Astronomy*, 41, 253
- Lovelace, R.V.E. & Romanova, M.M. 1996, in “Cygnus A – Study of a Radio Galaxy”, eds. C.L. Carilli & D.E. Harris (Cambridge: CUP), p.98
- Marcaide, J.M. & Shapiro, I.I. 1984, *ApJ*, 276, 56
- Marcaide, J.M., Shapiro, I.I., Corey, B.E., et al. 1985, *A&A*, 142, 71
- Marcaide, J.M., Elósegui, P., & Shapiro, I.I. 1994, *AJ*, 108, 368
- Marscher, A.P. 1980, *ApJ*, 235, 386
- Marscher, A.P. 1995, in *Publications of the National Academy of Sciences, Vol.92, Quasars and Active Galactic Nuclei: High Resolution Radio Imaging*, eds. M.H. Cohen & K.I. Kellermann (reprint: Charlottesville, NRAO), 11442
- Readhead, A.C.S. 1994, *ApJ*, 426, 51
- Rioja, M.J. & Porcas, R.W. 1997, in *Proceedings of IAU Colloquium No.164*, eds. J.A. Zensus, J.M. Wrobel & G.B. Taylor (Cambridge: CUP)
- Rybicki, G.B. & Lightman, A.P. 1979, “Radiative Processes in Astrophysics”, (J.Wiley: New York)
- Scheuer, P.A.G. 1960, *MNRAS*, 120, 231
- Sol, H., Pelletier, H. & Asséo, E. 1989, *MNRAS*, 237, 411
- Stevens, J.A., Litchfield, S.J., Robson, E.I., et al. 1996, *ApJ*, 466, 158
- Udomprasert, P.S., Taylor, G.B., Pearson, T.J., & Roberts, D.H. 1997, *ApJ*, 483, L1
- Unwin, S.C., Wehrle, A.E., Urry, C.M., et al. 1994, *ApJ*, 432, 103
- Unwin, S.C., Wehrle, A.E., Lobanov, A.P., et al. 1997, *ApJ*, 480, 596
- Vermeulen, R.C. & Cohen, M.H. 1994, *ApJ*, 430, 467
- Vermeulen, R.C., Readhead, A.C.S., & Backer, D.C. 1994, *ApJ*, L41.
- Walker, R.C., Romney, J.D., & Benson, J.M. 1994, *ApJ*, 429, L45
- Wardle, J.F.C., Cawthorne, T.V., Roberts, D.H., & Brown, L.F. 1994, *ApJ*, 437, 122
- Webb, J.R., Shrader, C.R., Balonek, T.J., et al. 1994, *ApJ*, 422, 570

Zensus, J.A., Cohen, M.H., & Unwin, S.C. 1995, ApJ, 443,
35
Zensus, J.A. et al. 1997, (in preparation)